

## **Development of a Novel Micro-CMM for 3D Micro/nano Measurements**

**K. C. Fan<sup>a,b</sup>, Y. T. Fei<sup>a</sup>, X. F. Yu<sup>a</sup>, Y. J. Chen<sup>a</sup>, W. L. Wang<sup>a</sup>, F. Chen<sup>a</sup> and Y.S. Liu<sup>a</sup>**

<sup>a</sup> **Department of Precision Instruments, Hefei University of Technology,  
Hefei 230009, P. R. China**

<sup>b</sup> **Department of Mechanical Engineering, National Taiwan University,  
1, Sec. 4, Roosevelt Rd., Taipei 10627, Taiwan  
fan@ntu.edu.tw**

<sup>b</sup>**Corresponding author:**

Kuang-Chao Fan, Email: [fan@ntu.edu.tw](mailto:fan@ntu.edu.tw);

Telephone: +886-2-2362-0032, Fax: +886-2-2364-1186.

## **Abstract**

A high precision Micro-CMM (Coordinate measuring machine) is under development. The expected measuring range is 25 x 25 x 10 mm and the resolution is 1 nm. In order to enhance the structural accuracy, some new design concepts are introduced, such as the arch-shape bridge for better stiffness and thermal accuracy, and the co-planar stage for less Abbe' error. The linear diffraction grating interferometer and subdivision technique is proposed for position sensing to nanometer resolution. The focusing probe on the laser interferometer feedback spindle is structured in the Z-axis to guarantee the nanometer stability. In this report, the detailed design principles of the developed Micro-CMM are described. The performance evaluation of each module of the prototype micro-CMM is presented. The positioning resolution of each axis to 1nm can be achieved by combining the coarse and fine motion control on a piezo-ceramic linear motor. The Z-axis measurement can be controlled to within 15nm repeatability. Parts of the positional accuracy of the co-planar stage have been achieved. Some problems due to current techniques will be addressed.

**Keywords:** Micro-CMM, nanometer accuracy, arch bridge, co-planar stage, focusing probe.

## **1. Introduction**

Technology of micro/nano 3-D profile measurement has received a great attention during the past decade [1]. Many fine components recently fabricated by micro system processes, such as MEMS, LIGA or micro machining, are in overall dimensions within meso scale and required accuracy from microns to tens of nanometers. Conventional coordinate measuring machines (CMM) are no longer capable of 3D measurements of these fine parts. Some advanced probes, such as SPM, are already commercially available but are only limited to 1-D sensing to nanometer resolution. Even equipped with PZT stages their measurement ranges are limited up to 100 $\mu$ m. It was noted by Takamasu [2] and Ni [3] that an overall consideration in the 3-D measurement system and its integration shouldn't be overlooked. Small sized CMMs have become a new topic of research, such as the Nano-CMM by Takamatsu [2], Small-CMM by NPL [4], Nanopositioning CMM by Hausottee and Jäger [5], Micro-CMM by Fan [6] and Liang [7], etc. There are also some micro scaled touch probe systems, such as the mechanical ball by Takamasu [8], MEMS by Eindhoven Univ. [9] and optical fiber by PTB [10], etc. Small CMM requires higher accuracy and resolution. Scaling down the conventional CMM design principle is not a feasible way as many existing mechanical components are all in micrometer accuracy. This paper presents an innovative micro-CMM design with the consideration of some completely new system modules, including the arch-shape bridge for better stiffness and thermal accuracy, the co-planar stage for less Abbe' error, the diffraction gratings with interferometric fringes and subdivision technique for nanometer resolution, and the focusing probe on the laser interferometer feedback spindle for the guarantee to nanometer stability. This Micro-CMM is designed for the measurement of meso-to-micro scale parts. It is aimed at achieving 1nm resolution and 30nm accuracy within a measuring range of 25x25x10mm. So far, the Z-axis measurement can be controlled to within 15nm repeatability. Parts of the objectives have been achieved. Some problems due to current techniques will be addressed.

## **2. System Configuration of the Micro-CMM Structure**

### **2.1 Concept of the arch-bridge structure**

Rectangular type of the bridge is always employed in the precision CMM structure for mounting the Z-axis probe, as shown in Fig. 1a. Although its static deflection does not

influence the measuring accuracy, the generated driving force and temperature rise from the motion actuator will, however, induce dynamic and thermal deformations of the bridge up to submicron level. In order to meet the high precision requirement in nanometer measurement, the conventional rectangular bridge shape has to be redesigned.

The deformation at the center of the bridge is very critical because of the concentrated load from the spindle and the generated driving force, which will react to the bridge. The maximum deflection at the center of the rectangular-bridge due to the spindle load  $P$  can be described as [15]:

$$\delta_{y \max} = 0.55 \frac{PR^3}{EI} \quad (1)$$

where,  $R$  is the half span of the bridge,  $E$  is the Young's modulus of the bridge material, and  $I$  is the moment of inertia of the cross section. During the spindle up and down motion a generated driving force of the actuator will impose a dynamic force ( $p$ ) on the bridge. The overall load on the bridge center will be  $(P + p)$ .  $p$  can be expressed by  $p \sin(2\pi ft)$ , where  $p$  is the amplitude of the dynamic force and  $f$  is the frequency.

This research proposes a fixed arch-bridge structure, as shown in Fig. 1b. Under the same dimension and the same spindle load, the maximum deflection at the center of the arch-bridge can be reduced to ( $R$  is the radius of the semi-circle bridge):

$$\delta_{y \max} = 0.24 \frac{PR^3}{EI} \quad (2)$$

The physical dimensions of the developed Micro-CMM bridge are: the outer radius is 220mm and the inner is 150mm; the width is 60mm and the dimension of the supporting pad is 70mm×100mm×40mm. It is made of granite material. The total weight is about 40kg. The spindle adds additional weight of about 3kg. Fig. 2 shows the deformed shapes of two bridges by finite element method. Table 1 lists the comparison between the analytical and FEM methods of two bridges.

(Insert Figs. 1 and 2, and Table 1 here)

From Table 1 we can clearly see that the Arch-bridge has higher stiffness than the

conventionally rectangular type to almost twice amount. Although the static stiffness does not influence the accuracy of static measurement, however, the imposed dynamic force will certainly impose dynamic deflection on the bridge during the spindle motion for the touch triggered or scanning measurement mode. The final dynamic force will still apply to the bridge at the spindle holding position. This research employs a piezo ceramic ultrasonic actuator (Nanomotion Co, Model SP-4) to drive the spindle motion at the lower position of the spindle, being a single load condition. Its maximum excited force at maximum acceleration is 15N. Actual motion will be, however, controlled at very low speed. Suppose the driving force is 1N, the corresponding dynamic Z-deflection at the spindle end will be 6 nm to the rectangular bridge, and 3 nm to the arch type, from ANSYS results.

With regard to the thermal deformation, the SP-4 generates heat due to its friction force. Experimental observation showed that for a two-hour low speed run of the SP-4 under normal ambient temperature of 23.5°C its surface temperature will increase 1°C. This temperature rise will result in the spindle expansion at the tip in the amount of 14.6nm for the rectangular bridge and 9.1nm for the arch bridge using the ANSYS analysis. Therefore, a well temperature controlled environment ( $20\pm 0.1^\circ\text{C}$ ) should be provided to reduce this thermal effect.

## **2.2 Concept of the Co-planar XY stage**

Conventional XY stage is normally stacked up by two linear stages composing of many components, such as ball screw, bearing, linear slide, etc. The Abbe' error of the lower stage is high and the components are all made in micrometer accuracy range only. More rigorous considerations should be taken into account when the XY stage is used to the micro/nano motion accuracy. An innovative co-planar stage is thus proposed in this study, as shown its sectioning view in Fig. 3. The top table is moved in the X-direction along the precision ground rods (or guideway) mounted onto the frame, and the frame is moved in the Y-direction along the precision ground rods of the base. The sliding surface of the moving part is mounted with a Teflon pad to reduce the friction. Four guiding rods are located in the same plane. With such a design, the Abbe' error in vertical direction can be significantly reduced. This is the essence of co-planar stage. In addition, there are no transmission components and the geometry is symmetrical, which ensures less random error and better static deformation under the same working conditions. Each axis motion is actuated by a motor from one side and detected by a position feedback system from the opposite side.

(Insert Fig. 3 here)

The whole stage is made of Invar steel so that the thermal deformation due to the driving heat can be significantly reduced. In order to minimize the moving weight, the static deformation, and the thermal deformation, a modified structure is redesigned. Fig. 4 shows the new table shape of which the V-flat guideway feature allows the free end to eliminate the reaction force from the corresponding rod and allows free expansion of the table due to the driving heat. From the Finite Element Analysis with ANSYS software it shows that at the table center the static deformation is about 0.13 $\mu$ m, and the thermal distortion is only 3.2nm assuming a 5 temperature rise at the driver. Similar modification is also made to the moving frame. The complete design of this Co-planar stage with minimum stress and weight condition is shown in Fig. 5, where the actuator and the position sensor will be described in the following sections.

(Insert Figs. 4 and 5 here)

### **2-3 The Driving system and feedback sensor**

In order to remain high motion accuracy, the coplanar X-Y stage and the Z-stage are all driven by ultrasonic motors (model SP-4 made by Nanomotion Co. [11]). The SP-4 system consists of the motor and a drive amplifier. These two components are combined to create the piezoelectric effect. This effect converts electrical field to a mechanical motion. The important role of operation is the 4 piezo ceramic elements. When the excited voltage is applying across the element in a precise sequence, the front tip of the piezo elements generates an elliptical motion with the frequency of 39.6 KHz. This elliptical motion then drives the stage by friction force to create linear motion of the stage, as shown in Fig. 6. This cyclic motion is called the AC mode motion with minimum step of 5nm. This ultrasonic motor also features a DC mode motion actuated by a DC voltage, which is proportional to even finer motion within 5 nm. Since the motor is tiny and easy to control it is suitable to small nanostages.

(Insert Fig. 6 here)

The position feedback of linear motion in each axis is detected by the principle of linear diffraction grating interferometer (LDGI) with a 1nm resolution, as shown in Fig. 7 [12]. The laser diode emits a linearly P-polarized laser beam with 635nm wavelength. The gratings will reflect with  $\pm 1$  diffraction beams to mirrors 1 and 2 respectively. Passing through respective PBS (2 or 3) each beam will change to P-beam again. The left arm beam changes to S-beam after it transmits through the half wave plate (H). After the quarter wave plate Q2, the two diffractive beams will be retarded to the left-circularly polarized and right-circularly polarized beams respectively. Again, passing through PBS5 and PBS6 the vectors of the electric field of the combined beams received by PD1 and PD2 will have 90 degree phase shift. The Doppler effects due to the motion of the grating will then shift the phase of each received beam with the wavelength proportional to the grating pitch. Meanwhile, the zero-order diffraction beam reflected from the gratings will be polarized to the S-linear beam so that it will not return to the laser diode to disturb its constant power.

(Insert Fig. 7 here)

The interferometer fringes always have three major errors: the DC shift difference, the electronic gain difference, and the phase orthogonal error of two sinusoidal output signals [16]. Before going to the subdivision technique for finer resolution and accuracy, these errors have to be removed. In this research, the DC shift was compensated by the summation of each signal and its inverse signal to obtain the zero DC voltage; the gain error was removed by adjusting the respective resistance of each signal board; and the orthogonal error of two signals was corrected by changing the outputs to their vector sum and subtraction. Fig. 8 shows the Lissajous plots of before and after error compensation. The output signals have been modified very well for further subdivision process.

(Insert Fig. 8 here)

With regard to the fringe subdivision technique, although there have been many methods proposed by various researches, such as the curve fitting [16, 17], signal modulation [18] and with CCD [19], this research developed a simple and quick method of triangulation form approximation by computing  $|\sin \theta| - |\cos \theta|$  from the output signals, as shown in Fig. 9. The complete cycle counting and directional sensing can be done by

conventional up/down counter. Only the incomplete cycles at the beginning and the end ( $X_0$  and  $X_1$ ) are to be interpolated. The calculation is as simple as linear interpolation. The approximated linearity is about 4%.

(Insert Fig. 9 here)

## **2-4 Spindle head design**

The spindle that carries the probe is moved along a short linear stage, which is driven by a PCLM and its motion is detected by a Laser Interferometer, as shown in Fig. 10. A counterweight is applied to balance the total mass center during the spindle motion. The laser beam is in line with the probe to observe the law of Abbe' principle. During the motion the position is recorded by the laser interferometer and stopped by probe at its focusing point onto the object surface.

(Insert Fig.10 here)

## **3. Development of a focusing probe**

This research aims at development of a low cost optical probe with the measurement capability in the nanometer range [13]. The pickup head of the commercial DVD player was adopted based on its principle of focus error. As shown in Fig. 11. A 635 nm wavelength light source generated from a laser diode is primarily polarized by a grating plate. Passing through a beam splitter and a quarter wave plate the light beam is focused by an objective lens onto the object surface with a spot size approximately 1  $\mu\text{m}$  in diameter. The reflected beam signal is imaged onto a four-quadrant photo detector through the quarter wave plate. The quadrant detector outputs are combined to give a focus error signal (FES). In this system the focusing signal is detected by the Astigmatic method. At the focal plane the spot is a pure circle. When the object moves up or down away from the focal plane, the spot appears an elliptical shape in different orientations. The corresponding FES provides an S-curve signal proportional to the distance, as shown in Fig. 12. The linear range of the S-curve will vary according to the object's surface reflectivity. The higher the reflective surface the larger the linear range will be.

(Insert Figs. 11 and 12 here)

#### **4. Experimental Tests**

The developed Micro-CMM has been fabricated in components and integrated into a prototype machine. Fig. 13 shows the complete design and Fig. 14 is the prototype of the developed Micro-CMM. Some performance tests have been carried out.

(Insert Figs. 13 and 14 here)

##### **4-1 Environment effect**

Concerning the measurement in nanometer scale the environmental effect is very critical to the measured data. For the reference length using laser interferometer the temperature variation is the most important factor. This study was carried out in a temperature controlled room. Current facility can, however, provide only up to  $20\pm 1^\circ\text{C}$  temperature control. Two types of laser interferometers were employed, one is the HP5529A and the other one (Model PT-1002A) is made by Pretios Co. of China [20]. Both readings showed apparent drifts after warm-up and became stably fluctuated after 3 hours. A stability test was then carried out to see the readings at every 10 seconds for 1800 seconds. Fig. 15 shows that the HP5529A fluctuates between 60nm to -20nm, and PT-1002 varies between 18nm to -30nm. These results are all not satisfied yet. The environment control should be stricter.

(Insert Fig. 15 here)

##### **4-2 Positioning accuracy tests**

The motion of each axis, detected by the LDGI system, was calibrated using the HP5529A laser interferometer in a temperature controlled room ( $20\pm 1^\circ\text{C}$ ). For the long travel test, the AC mode of the ultrasonic motor was actuated. The positioning accuracy is below  $0.1\mu\text{m}$  in average with  $0.3\mu\text{m}$  standard deviation over 25mm, as shown in Fig. 16. It is still far beyond the required 30nm accuracy. Some possible error sources were found as follows:

- (1) The straightness polish of the guideway contact was not satisfied yet. The induced variable friction forces yielded to unsteady motion, which caused the noisy signals of the LDGI output.
- (2) The quality of the holographic gratings is also of the major concern. This study tried with two kinds of glass gratings from different makers. One is in 25mmx25mm size

and cut into three pieces, with 8mmx25mm each. The other one has 12.5mmx25mm grating surface. The uniformity of the grating pitch and the depth will influence the diffraction effect and will accordingly alter the DC drift and amplitude of the sinusoidal signals. In addition, improper cutting process of the glass gratings creates scratches

- (3) The quality of the optics, especially the PBS, is essential to the orthogonality of sine and cosine waveforms.
- (4) The stability of ambient temperature and the ground vibration are also the impact factors to the system accuracy.

(Insert Fig. 16 here)

For the medium travel test, it conformed to the ISO230-2 standard of NC machine tool positioning test. The travel was 5mm with 1mm steps for bi-direction motions in a selected middle region. The results are shown in Fig. 17. Although the accuracy could approximately be controlled within 30nm the error variation was still large. Again, the temperature effect could be the major source, which not only varies the LDGI readings but also the laser interferometer.

(Insert Fig. 17 here)

For the fine motion test of 1mm travel with 100 $\mu$ m steps for four runs, the averaged error could possibly fall into 30nm range with only one exception, as shown in Table 2. Since the tested position was specially selected, the error sources of long travels were not existed because there was no missing pitch count of the gratings. However, although the lasting time of this test was short, the variation of the HP laser interferometer readings could not be eliminated. The temperature variation might dominate the errors.

(Insert Table 2 here)

### **4-3 Focus probe test**

The focus error signal (FES) test was carried out by mounting the probe on a linear stage. The stage motion was measured by a laser interferometer. Fig. 18 shows the tested results

with respect to different materials. Good S-curve occurs when the material has good reflection surface [14].

(Insert Fig. 18 here)

#### **4-4 Spindle motion tests**

A small piece of mirror was mounted onto the table top of the co-planar stage as an object. Initially, the spindle was moved to focus the probe beam right on the mirror surface so that the FES output zero voltage. The spindle was then moved away with a random distance approximately 0.1 mm each time and returned back until the FES was zero again. The PT-1002A laser interferometer was mounted to detect the spindle motion. The readings of the laser interferometer at each focus positions showed quite a good repeatability within 15 nm for 12 runs, as shown in Fig. 19. As indicated in Fig. 15 that the PT-1002A has smaller fluctuation with time span, the spindle motion is quite successful and reliable.

(Insert Fig. 19 here)

### **5. Concluding Remarks**

This article states the current progress on the development of a Micro-CMM. Design considerations and preliminary results are described. With the particular consideration in the structural accuracy, the innovative arch-bridge and the co-planar stage are proposed. Equipped with the SP-4 ultrasonic actuator and the LDGI feedback system the motions in X and Y directions can achieve to 1nm resolution, same as to the Z-spindle motion mounted with the focus probe when driven by SP-4 and detected by PT-1002A laser interferometer. Experimental tests have shown that the Z-axis and the fine motion of the co-planar stage can meet the required accuracy of below 30nm. The medium and long motions of the co-planar stage are still not accurate enough. Some possible error sources are addressed. The whole software system of this prototype Micro-CMM is developed in the LABVIEW environment. Current work has not completed the system integration and tuning process. Continued works will focus on the improvement of the straightness of the guide way by harder workmanship, the proper selection of the holographic gratings as well as the optics for better output signals, and the construction of a mini chamber to protect the system environment. Moreover, the volumetric errors of the CMM have to be calibrated and compensated in order to achieve higher accuracy. In addition, the miniature contact

probe will be studied.

### **Acknowledgements:**

The present authors gratefully acknowledge the support provided to this project by the National Natural Science Council of China under Contract No. 50275048 and 50420120134, and the National Science Council of Taiwan under Contract No. 942212E002001.

### **References**

1. McKeown, P. "Nanotechnology-Special article," Proc. of the Nano-metrology in Precision Engineering, Hong Kong, pp. 5-55, Nov. 24-25, 1998.
2. Takamasu, K., Guo, B. W., Furutani, R. and Ozano, S. "Basic Concept of Feature-based Metrology," Proc. of the 6<sup>th</sup> ISMQC Symposium, Vienna, 1998.
3. Ni, J. "Future direction of micro/meso-scale manufacturing," invited speech, Proc. of the 6<sup>th</sup> ICFDM'2004, Xi'an, China, June 21-23, 2004
4. Peggs, G. N., Lewis, A. and Leach, R. K., "Measuring in Three Dimensions at the Mesoscopic Level," Proceedings of the ASPE Winter Topical Meeting - Machines and Processes for Micro-scale and Meso-scale Fabrication, Metrology and Assembly., Florida, USA, January 2003, 53-57.
5. Hausottee, T., Jäger, G., et al., "Traceable Nanometrology with a Nanopositioning and Nanomeasuring Machine," J of CSME, Vol. 25, No. 5, 2004, pp. 399-404.
6. Fan, K. C., Chu, C. L., Chang, S. H. and Chung, T. T., "Development of a micro-CMM for Nanometrology," Proceedings of KSPE Spring Conference, Keynote paper, pp. 1-6, 2001.
7. Liang, S. "Machining and metrology at micro/nano scale," keynote speech, Proc. of the 1<sup>st</sup> ICPT, Hamamatsu, Japan, June 9-11, 2004.
8. Enami, K., Hiraki, M. and Takamasu, K., "Nano probe using optical sensing," XVI IMEKO World Congress, IMEKO 2000, Wien, Austria, September, 2000.
9. Haitjema, H., Pril, W.O. and Schellekens, P., "Development of a Silicon-based Nanoprobe System for 3-D Measurements," Annals of the CIRP, 50 (1), pp. 365-368, 2001.
10. Schwenke, H., Härtig, F., Wendit, K. and Wäldele, F., "Future Challenges in Co-ordinate Metrology: Addressing Metrological Problems for Very Small and Very Large Parts," IDW Conference, Knoxville, pp. 1-12, May 2001.

11. Pohl, D. W. "Dynamic Piezoelectric Translation Devices," *Rev. Sci. Instrum.*, Vol. 58, No. 1, pp. 54-57, 1987.
12. Fan, K. C., "A high precision diffraction interferometry stylus probing system," keynote paper, Proc. of ICMT, Kitakyushu, Japan, 2002.
13. Fan, K.C., Chu, C.L. and Mou, J. I., "Development of a Low-Cost Autofocusing Probe for Profile Measurement," *Measurement Science and Technology*, Vol. 12, pp. 2137-2146, 2001.
14. Fan, K. C., Lin, C. Y. and Shyu, L. H., "Development of a Low-cost Focusing Probe for Profile Measurement", *Measurement Science and Technology*, Vol. 11, No. 1, pp. 1-7, 2000.
15. Fan, K. C., Wang W. L. and Chen, F., "Innovative design of a new CMM bridge," *Chinese Journal of Mechanical Engineering*, 2004, (in press).
16. Heydemann, P.L.M., "Determination and correction of quadrature correction of fringe measurement errors in interferometers," *Applied Optics*, 20, 1981, pp. 3382.
17. Birch, K. P., "Optical fringe subdivision with nanometric accuracy," *Precision Engineering*, Vol. 12, No. 4, pp. 195-198, 1990.
18. Chen, B. Y. and Li, D. C., "Progress in Studies on Long-Range and Ultrahigh-Accuracy Nanometer Measurements," *Proceedings of the 2<sup>nd</sup> ISIST*, Vol. 2, Jinan, China, 2002, pp. 84-89.
19. Wen, P. and Hsu, D. H., "Direct subdivision of Moire fringe with CCD," *Proceedings of SPIE*, Vol. 1230, 1990, pp. 165-166.
20. Pretios Co., [http:// www.pretios.com](http://www.pretios.com), Beijing China, 2005.

Table 1: Comparison between Rectangular-bridge and Arch-bridge ( $\mu\text{m}$ )

Deflection	Analytical solution with spindle load	FEA	
		Spindle load	Self-weight
Rectangular	0.398	0.362	0.156
Arch-bridge	0.197	0.174	0.102

Table 2: Positioning accuracy of fine motion (nm)

Distance (mm)	Error1	Error2	Error3	Error4	$\overline{\text{Error}}$	$\sigma$
0	0	0	0	0	0	0
0.1	-5	-13	-17	-10	-11.2	5.1
0.2	-19	-32	-27	-28	-26.5	5.5
0.3	-27	-8	-26	-33	-23.5	10.8
0.4	-34	-33	-33	-26	-31.5	3.7
0.5	-11	-14	-20	-13	-14.5	3.9
0.6	0	-11	-20	21	-2.5	17.7
0.7	17	2	-16	4	1.7	13.6
0.8	27	4	3	32	16.5	15.1
0.9	14	15	5	23	14.3	7.4
1	7	29	19	4	14.8	11.5

## Figure captions

Figure 1: (a) the rectangular bridge, (b) arch-bridge.

Figure 2: Deformed bridges by FEM analysis, (a) rectangular, (b) arch

Figure 3: Proposed symmetrical co-planar XY-stage

Figure 4: Modified guide way shape of the table

Figure 5: Final stage design of minimum stress and weight

Figure 6: Motion principle of the ultrasonic motor

Figure 7: Principle of linear diffraction interferometer (LS: laser diode, L: lens, S: stage, G: grating, PBS<sub>i</sub>: *i*th polarizing beam splitter, M<sub>i</sub>: *i*th mirror, NPBS: non-polarizing beam splitter, Q<sub>i</sub>: *i*th quarter wave plate *i*, PD<sub>i</sub>: *i*th photo detector).

Figure 8: The Lissajous plots of before and after error compensation.

Figure 9: Signal subdivision method

Figure 10: The spindle head design (1-probe tip, 2-PCLM, 3-linear stage, 4-counterweight, 5-probe head, 6-laser beam, 7-interferometer, 8-laser head).

Figure 11: Principle of the focusing probe

Figure 12: The variation of the spot shape with the S-curve.

Figure 13: The structure of innovated Micro-CMM

Figure 14: The prototype Micro-CMM

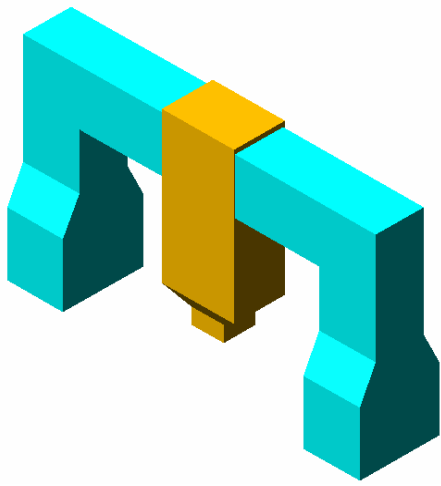
Figure 15: Stability tests of two laser interferometers

Figure 16: Long travel positioning accuracy of one axis

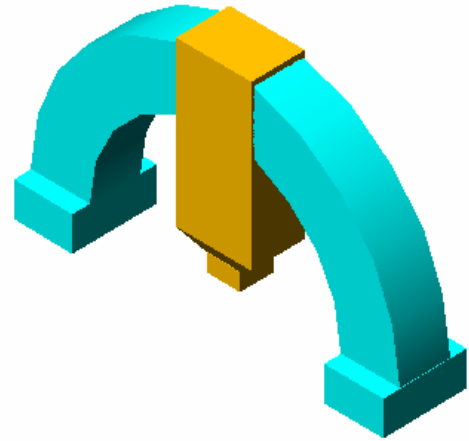
Figure 17: Fine motion positioning accuracy of one axis

Figure 18: S-curves for various materials

Figure 19: Repeatability test of spindle and probe system

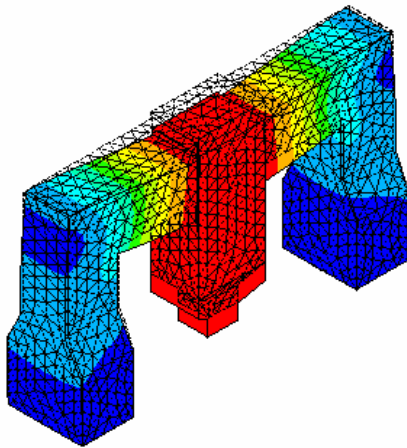


(a)

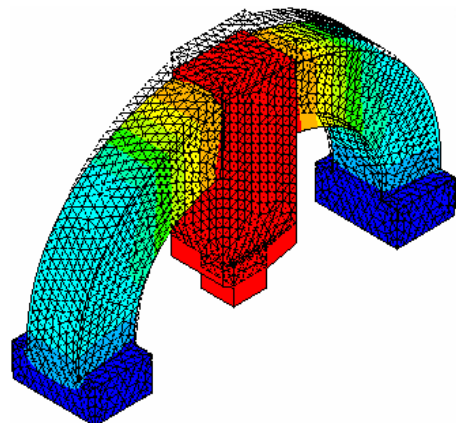


(b)

Figure 1



(a)



(b)

Figure 2

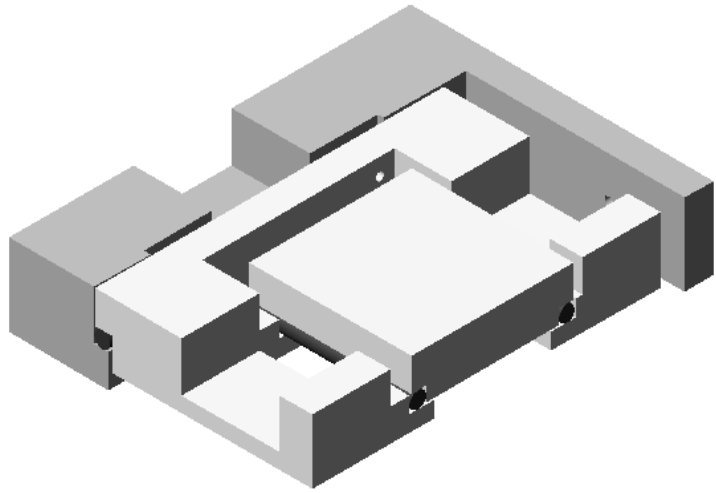


Figure 3

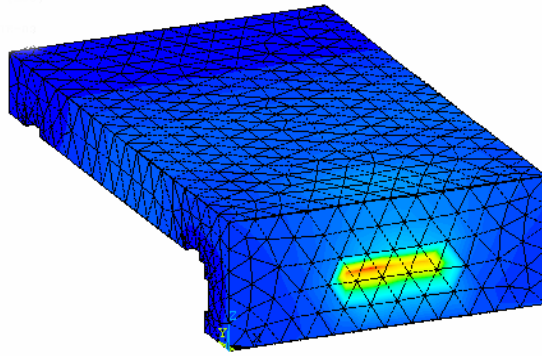


Figure 4

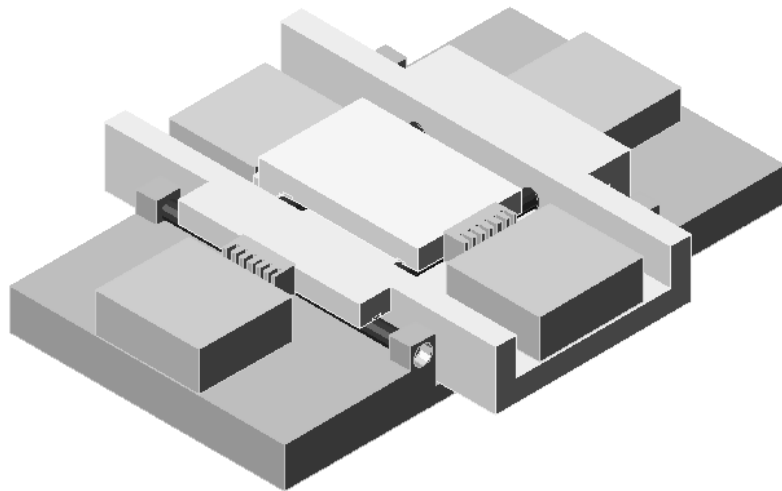


Figure 5

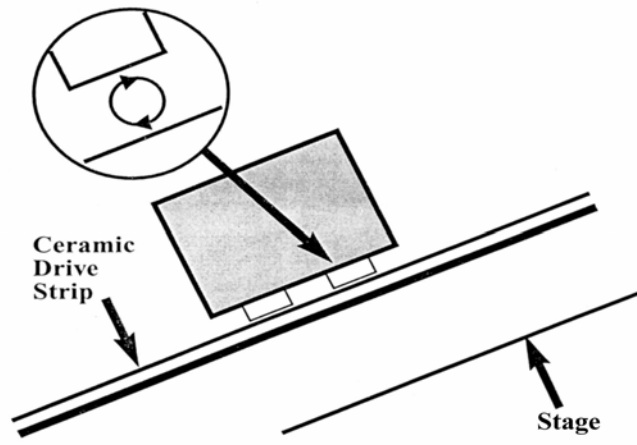


Figure 6

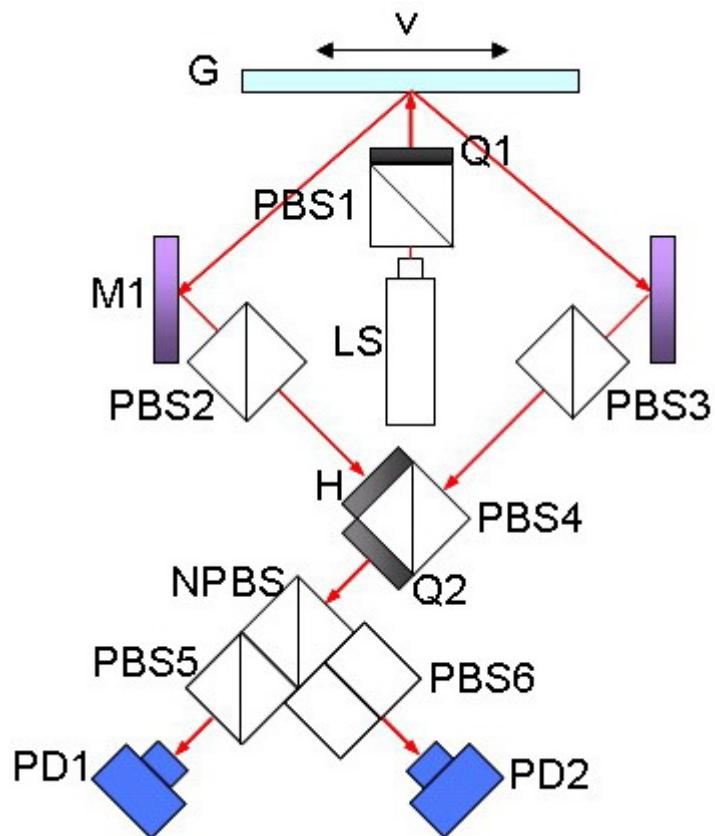


Figure 7

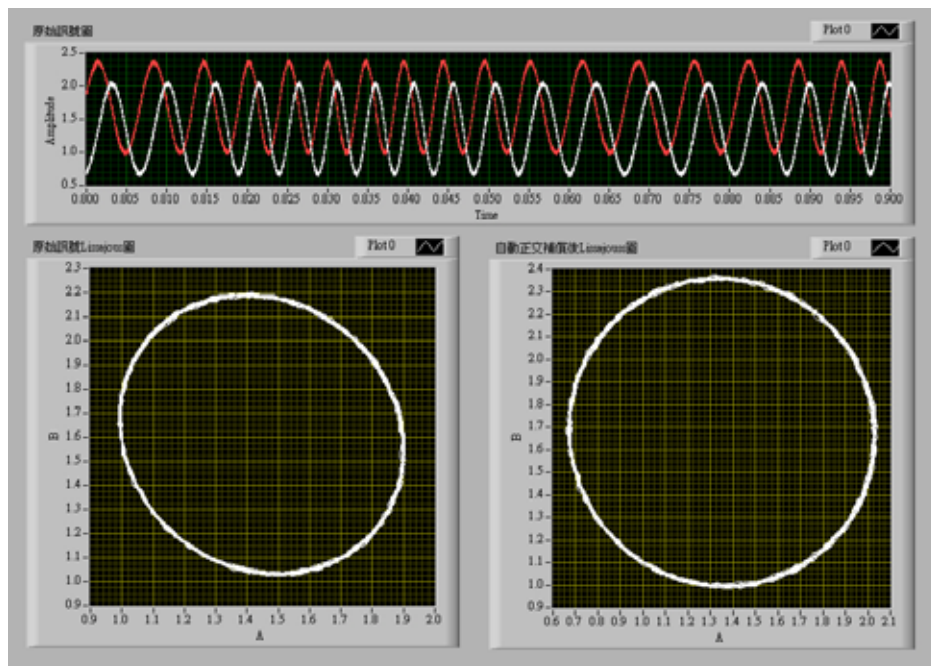


Figure 8

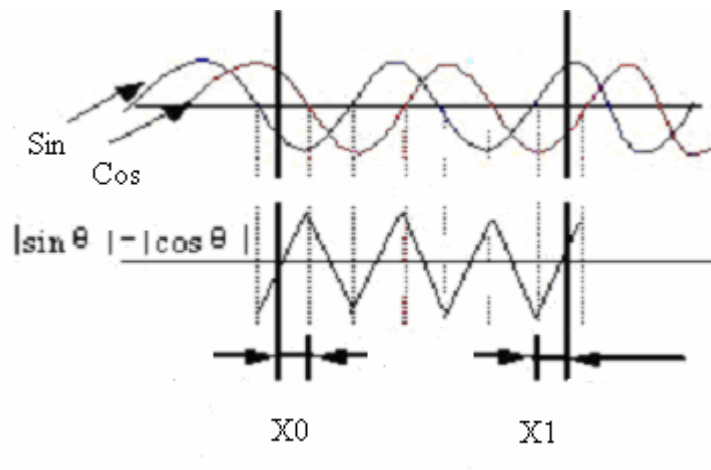


Figure 9

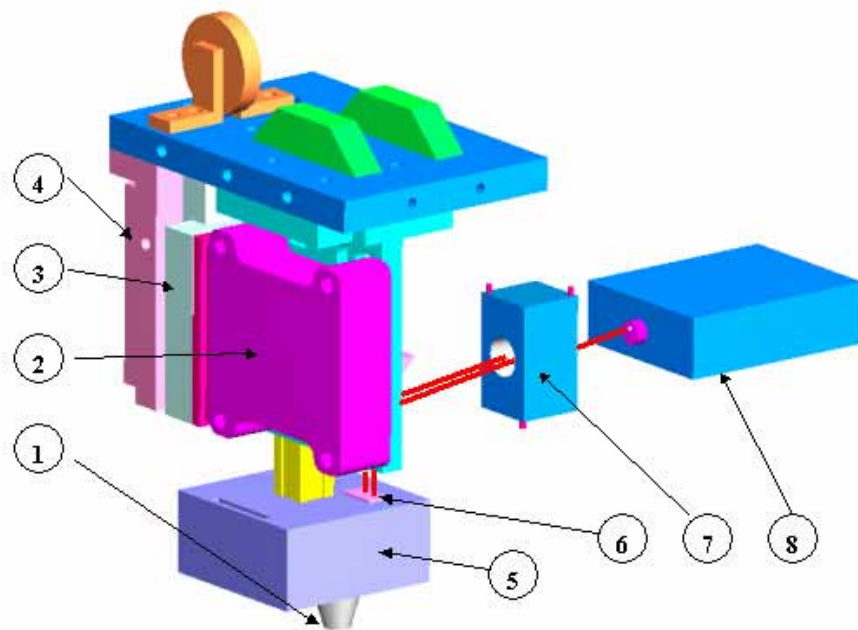


Figure 10

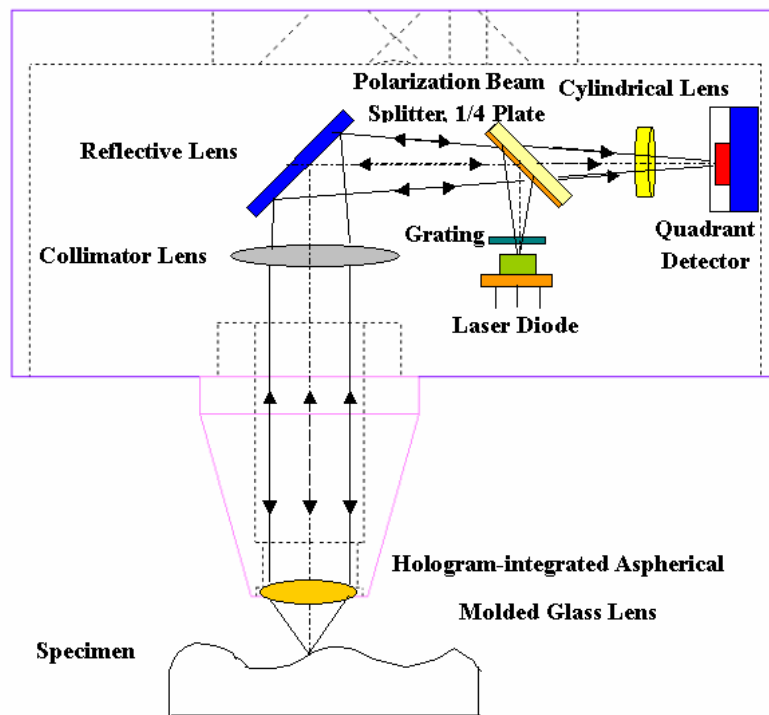


Figure11

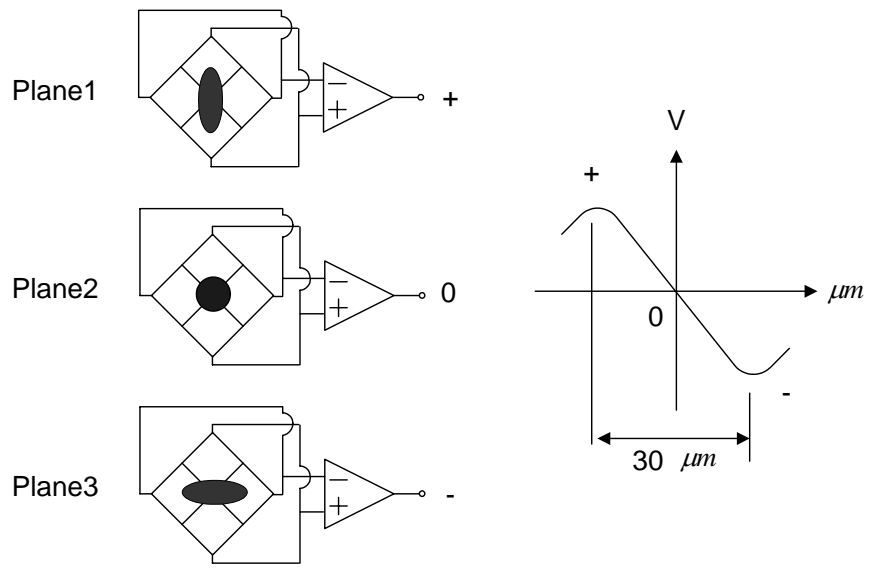


Figure 12

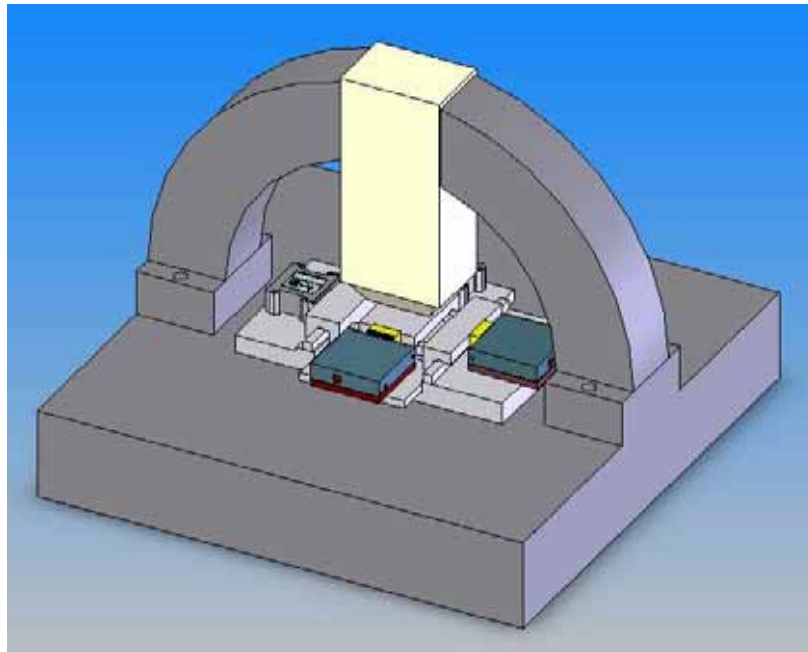


Figure 13

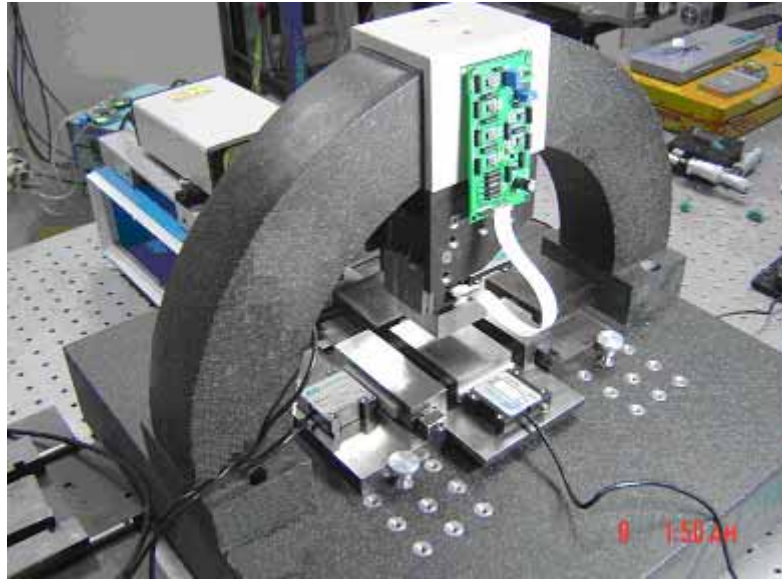


Figure 14

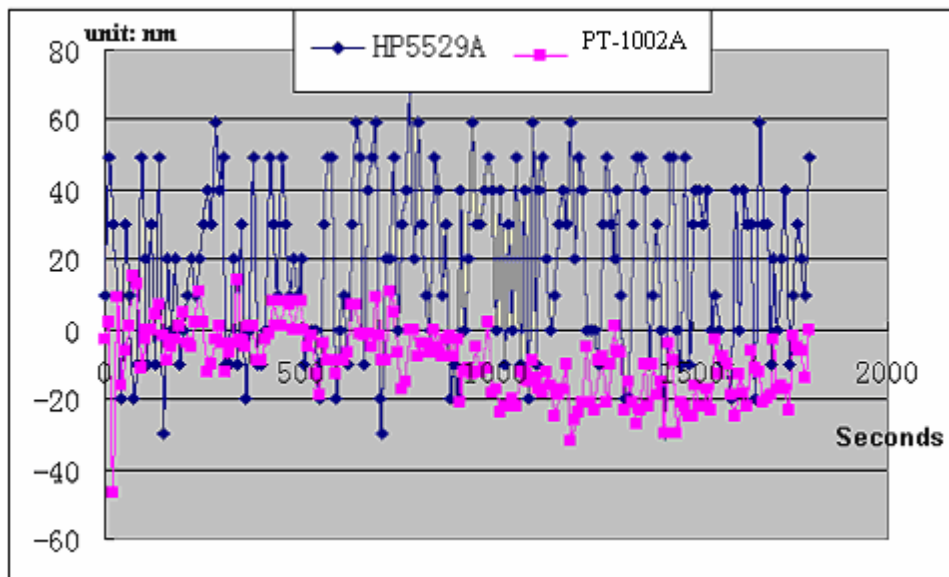


Figure 15

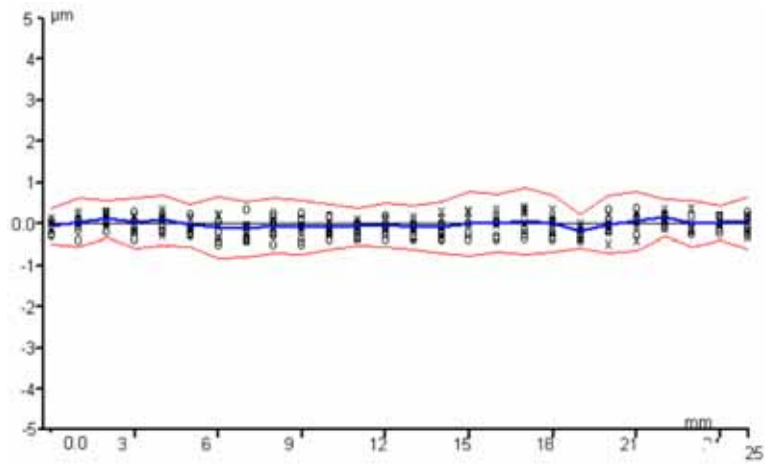


Figure 16

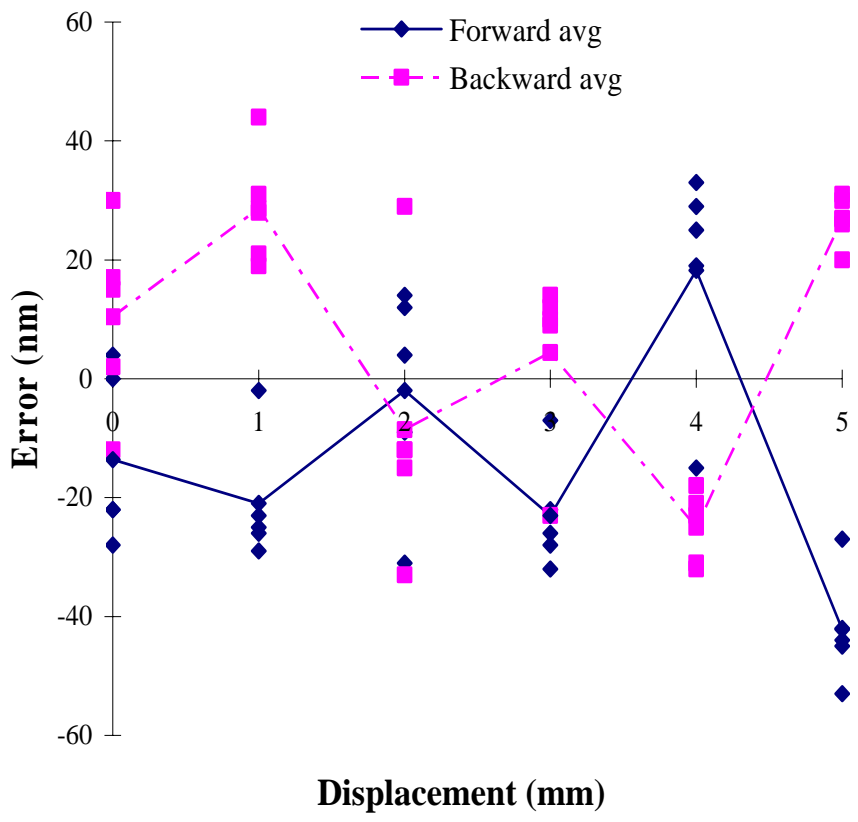


Figure 17

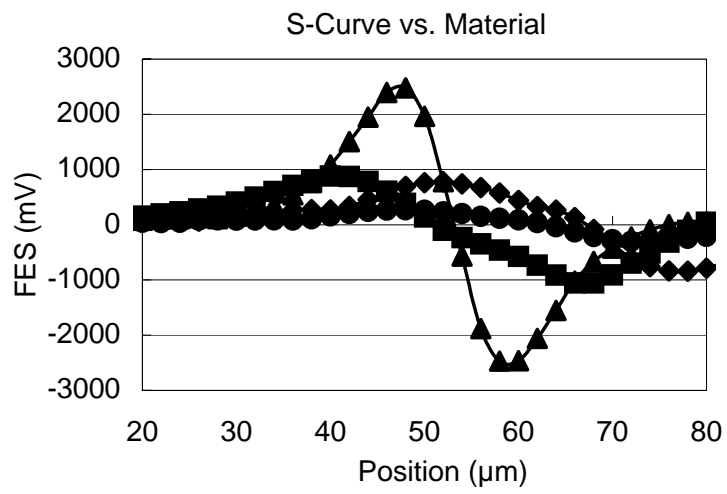


Figure 18

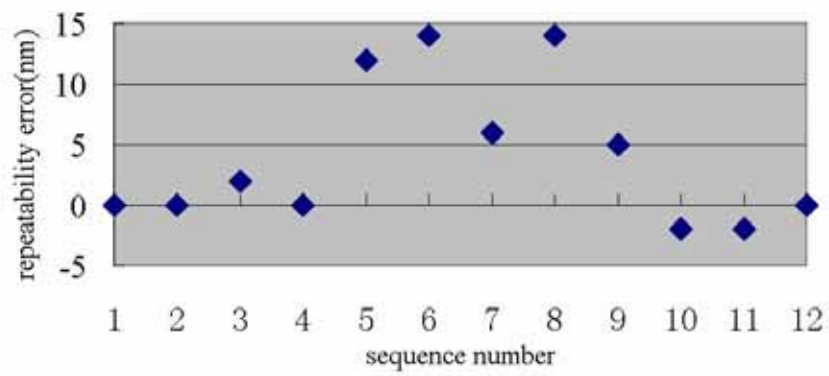


Figure 19